# Influence of deformability behavior in prestressed concrete beams using carbon-fiber-reinforced polymer tendon

P. Selvachandran, S. Anandakumar, and K. L. Muthuramu

- Premature failure can occur in prestressed concrete beams due to nonductile behavior of carbon-fiber-reinforced polymer (CFRP) tendons.
- This article assesses the influence of deformability behavior in flexure and serviceability properties of CFRP prestressed concrete beams.
- Performance of prestressed CFRP beams was assessed by experimental investigation.

A major challenge in the precast/prestressed concrete industry is premature failure of beams due to corrosion in steel tendons. Hence, the use of fiber-reinforced polymer (FRP) tendons in the construction industry is growing despite their limitations compared with steel tendons. FRP materials are strong, light, and noncorrosive but perform poorly with regard to creep and ductility. FRP's stress–strain curve is linear; however, FRP prestressed concrete beams deviate from this linear relationship beyond service loads. This is because the beam absorbs some strain energy, which can be measured as deformability behavior of an FRP prestressed concrete beam. The strain ratio at ultimate stage to service stage of the FRP tendon is less than that of a steel tendon.

Burke and Dolan[1,2] suggest a simplified method for calculating the deformability of FRP prestressed beams that uses a strain approach. American Concrete Institute (ACI) 440.4R-04[3] amends the strain approach. Deformability is measured in terms of deformability index *DI* and is defined as the ratio of ultimate strain $\varepsilon_{pu}$ to prestressing strain $\varepsilon_{ps}$ at service stage with the modification due to difference in the neutral axis of elastic and inelastic behavior.

$$DI = \frac{(1-k)\varepsilon_{pu}}{1-\frac{\alpha}{d\beta_1}\varepsilon_{ps}}$$

where

$k$ = ratio of neutral axis depth to effective depth

$\alpha$ = rational parameter = $\dfrac{\rho d f_{pu}}{0.85 f_c^{'}}$

$d$ = effective depth

$\beta_1$ = stress block factor for concrete

$\rho$ = reinforcement ratio

$f_c^{'}$ = compressive strength of concrete

Burgoyne[4] states that beam deformability influences the moment-curvature graph, which improves the behavior of the beam in terms of flexure and serviceability.

This paper presents the findings of an experimental investigation on the influence of deformability behavior in carbon-fiber-reinforced polymer (CFRP) prestressed concrete beams. Experimental results were compared with ACI 440.4R-04 design recommendations, the existing literature, and proposed design modifications to improve performance. In order to study beam deformability behavior, the other influencing parameters were not varied. Good bonded condition of the prestressing tendon without nonprestressed steel at the tension side was considered for the experimental investigation.

## Experimental program

Four beam specimens were cast with varying levels of prestressing in the CFRP tendon and were then tested in a laboratory.

### Test specimen and setup

The beam specimens are rectangular with dimensions of 150 × 250 mm (5.9 × 9.8 in.) and 3100 mm (122 in.) long. The beams were cast with void former using polyvinyl chloride (PVC) pipe and grout tubes to facilitate the placing of posttensioning rods and grouting after stressing the tendon. After the initial setting of concrete, the PVC pipe and tube were removed. A CFRP tendon used as a posttensioned rod was placed as a straight tendon and stressed to 35% to 70% of ultimate load. **Figure 1** shows the simply supported beams with two-point loads considered in this study. The beam specimen was designed as a tension-controlled member. The top reinforcement was considered as a hanger bar to support shear links, and there are no nonprestressed reinforcements provided at the bottom. Shear stirrups made of 8 mm (0.3 in.) diameter bars spaced at 150 mm (5.9 in.) were designed to avoid shear failure during testing. The sandy surface of the tendon was polished using sandpaper, and a strain gauge strip was attached to the surface of the CFRP rod to measure the strain during prestressing. Three dial gauges were mounted at the bottom of the beam to measure deflection during testing (Fig. 1). One dial gauge was located at midspan, and the other two dial gauges were 500 mm (20 in.) to the left and right of midspan. Pellets were fixed on the sides faces of the beam (in the midspan zone) for 1 m (3.3 ft) in length to measure the change in the curvature of the beam during loading. Pellets were fixed at an interval of 100 mm (4 in.) wide and 50 mm (2 in.) tall. Demountable mechanical strain gauges were used to measure the strain at each pellet node.

### Test matrix

Four CFRP prestressed beam specimens were considered, with the following percentages of effective prestress applied: 35%, 48%, 61%, and 70%. The position and number of CFRP tendons were also varied to study the behavior of beams with different conditions. Figure 2 shows the experimental beam specimen configurations. In the specimen nomenclature, B1 is the specimen number, 2 is the number of tendons, H signifies horizontal (V is for vertical), and 0.61 is the percentage of effective prestress.

### Material properties

The concrete mixture was designed for a cylinder compressive strength of 40 MPa (5.8 ksi) and a cube compressive strength of 50 MPa (7.2 ksi) and was confirmed by trial mixture test results. Nine cube and cylinder specimens were cast and tested at the time of stressing and testing of the beams. The average test results achieved at 7 days and 28 days for the concrete cube compressive strengths were 50.8 and 61.3 MPa (7.37 and 8.89 ksi), respectively, and tensile strength were 3.4 and 4.56 MPa (0.49 and 0.66 ksi), respectively. The modulus of elasticity of concrete derived from the test results were 37.7 and 38.6 GPa (5470 and 5600 ksi) for 7 and 28 days, respectively. CFRP bars with a diameter 9.5 mm (0.37 in.) and an area of 71.3 mm$^2$ (0.111 in.$^2$) were used in this investigation. The tensile strength of CFRP bars was 1896 MPa (275.0 ksi) for the ultimate strain of 0.0153 and the modulus of elasticity was 124 GPa (17,984 ksi). Both ends of the CFRP tendon were connected with a splicer to protect the surface of the tendon during stressing. The tensile strength of the steel hanger bar and stirrups was 500 MPa (73 ksi) for the yield strain of 0.0025, and the Young's modulus was 200 GPa (29,000 ksi).

### Prestressing of CFRP tendons

Johnson[5] adopted special measures to protect the surface of the CFRP tendons during stressing and anchorage. A similar system was adopted for this study (Fig. 1). Both ends of the beam specimen were connected with steel plates that were 100 × 150 mm (4 × 5.9 in.) and 24 mm (0.94 in.) thick to transfer the stress uniformly on both sides of beam.

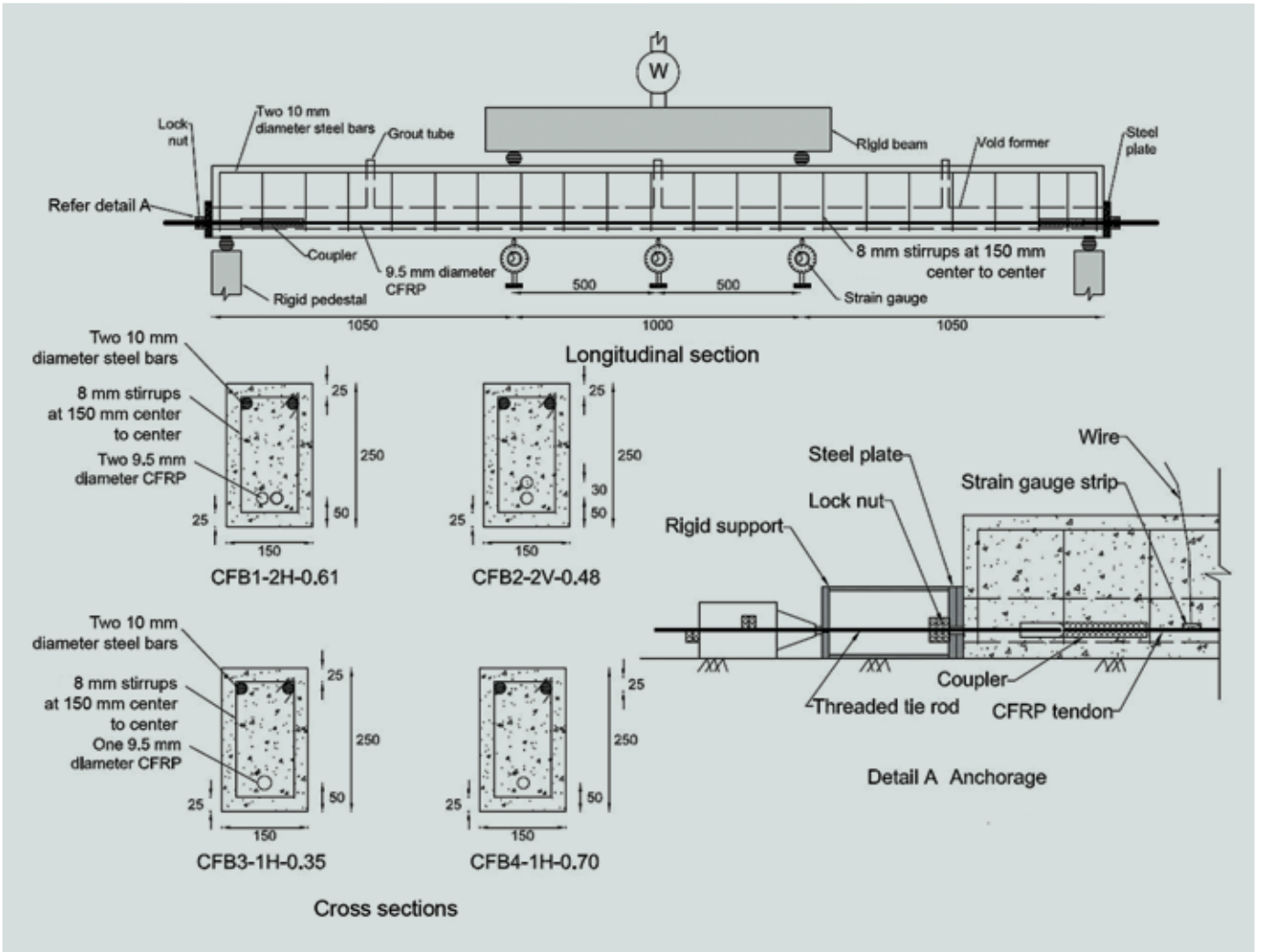


**Figure 1.** Beam configurations. Note: All measurements are in millimeters. 1 mm = 0.0394 in.

Threaded studs were connected to both ends of the CFRP tendon to connect to a hydraulic jack for stressing. Schmidt et al.[6] suggested clamping the anchor by bolting. Hence, a similar approach was adopted of providing high-strength nuts in threaded studs to lock the stress after posttensioning the tendons. A hydraulic jack with 99.64 kN (22.40 kip) capacity was used for stressing the CFRP tendon. The prestressing force on the tendon was attained by controlling the elongation of the tendon during stressing. Total elongation of the tendon and strut $\delta$ was determined by the following equation.

$$\delta = PL/(AE_p) = \delta_1 + \delta_2 + \delta_3$$

where

$P$ = prestressing load

$L$ = length of CFRP tendon

$A$ = area of CFRP tendon

$E_p$ = Young's modulus of carbon-fiber-reinforced polymer tendon

$\delta_1$ = elongation of stud

$\delta_2$ = elongation of CFRP tendon

$\delta_3$ = elongation of stud

Strain gauge strips attached to the prestressing bar were used to measure the actual strain in the tendon. Immediately after stressing the tendon, the cement grout was placed through the grout tube. The loss of strain in the tendon was measured by the strain gauge before load was applied to a member. Tendon slip and transfer length were measured and the tendon was considered in elongation. The effective prestressing force was calculated after considering all strain loss, as suggested by Tadros et al.[7] **Table 1** shows the effective prestressing force and corresponding elongation achieved.

**Table 1.** Prestressing force and midspan deflection of beam

| Beam type | Elongation, mm | | Effective stressing force, kN | Deformability index *DI* | Deflection at ultimate load, mm | |
|---|---|---|---|---|---|---|
| | $\delta_2$ | Due to loss of stressing | | | Experimental | ACI 440.4R-04 |
| CFB1-2-H-0.61 | 30 | 3 | 164.8 | 1.83 | 39 | 31.9 |
| CFB2-2-V-0.48 | 24 | 2.75 | 129.7 | 2.36 | 44 | 40.2 |
| CFB3-1-H-0.35 | 18 | 2.4 | 47.5 | 2.88 | 34.80 | 30.95 |
| CFB4-1-H-0.70 | 34 | 3 | 94.5 | 1.36 | 22.0 | 11.8 |

Note: $\delta_2$ = elongation of carbon-fiber-reinforced polymer tendon. 1 kN = 0.225 kip.; 1 mm = 0.0394 in.

## Beam specimen testing

A two-point load test was conducted for beam specimens CFB1 to CFB4 on the 498.2 kN (112.0 kip)–capacity test frame. The simply supported beams were loaded in increments of 5 kN (1.1 kip) until the first crack appeared in the beam. The load increment was then reduced to 2.5 kN (0.56 kip) during the cracking stage. A load cell was used to measure the applied load and control the increment of load. Three dial gauges were also used to measure the deflections during testing. Demountable mechanical gauges were used to measure the strain in the midspan zone of 1 m (3.3 ft). Crack meters were used to measure crack widths. Deflections and crack widths were recorded for each load increment.

## Experimental test results and discussion

## Flexural behavior

The flexural behavior of a member is measured based on the cracking moment and final failure type at ultimate load. The failure type is either rupture of the tendon or compression of the concrete. The experimental cracking moments were approximately the same as the theoretical calculations using the ACI 440.4R-04 method (**Table 2**), hence the effectiveness of prestressing the tendon and the concrete strength of the beam are achieved as per design calculations. The failures of beam specimens were observed as ruptures of CFRP tendons, which resemble the design consideration of tension-controlled members.

A load–deflection curve (**Fig. 2**) was plotted for beam specimens CFB3 (35% prestress) and CFB4 (70% prestress). A beam with a high percentage of prestress provides a greater cracking moment than a beam with a low percentage of prestress; however, the ultimate moment is almost equal for both cases. The failure loads at the ultimate moment of the beams are almost equal. This shows that the deformability behavior of CFRP tendons does not influence the flexural strength of the member. However, the graph of moment curvature did change with respect to the deformability behavior of the prestressed beam. Swanson and Dolan[8] also predicted the moment curvature changes with respect to the deformability behavior of the member. The experimental ultimate moment is less than the theoretical calculation, hence the multiplication of the utilization factor as suggested by ACI 440.4R-04 should be used to predict the design ultimate moment.

## Serviceability behavior

**Deflection** The load–deflection behavior of a member is not perfectly elastic despite the fact that CFRP materials' stress–strain curve is linear to failure. The experimental

**Table 2.** Moment

| Beam type | Cracking moment $M_{cr}$, kN-m | | | Ultimate moment $M_n$, kN-m | | |
|---|---|---|---|---|---|---|
| | ACI method | Experimental | Test/ACI method | ACI method | Experimental | Test/ACI method |
| CFB1-2-H-0.61 | 21.8 | 22.5 | 1.03 | 45.8 | 44.45 | 0.97 |
| CFB2-2-V-0.48 | 18.2 | 17.5 | 0.96 | 44.1 | 43.5 | 0.98 |
| CFB3-1-H-0.35 | 10.6 | 11.25 | 1.06 | 25.8 | 25.1 | 0.97 |
| CFB4-1-H-0.70 | 16.0 | 16.5 | 1.03 | 25.2 | 25.2 | 0.99 |

Note: 1 kN-m = 0.738 kip-ft.

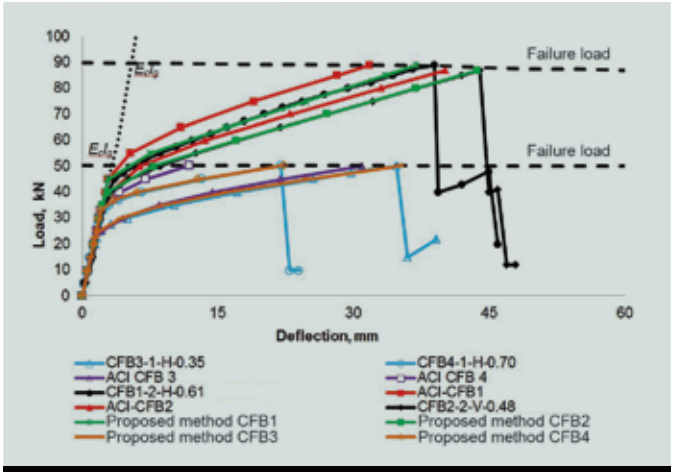


**Figure 2.** Load–deflection curve of concrete-fiber-reinforced polymer prestressed concrete beam. Note: $E_c$ = Young's modulus of concrete; $I_g$ = gross moment of inertia of member. 1 mm = 0.0394 in.; 1 kN = 0.225 kip.

test results showed that during unloading of beams within service load, the deflection does not change at the same rate as the loading. Table 1 shows the ultimate deflection values of the tested beams. The ultimate deflections gradually increased with the increased deformability index value. The deflection of the beams converged faster during the cracking stage for the beams with a higher percentage of prestressing than those with a lower percentage of prestressing. The load–deflection curve (Fig. 2) reveals that the 35% prestressed beam deformed better than the 70% prestressed beam. This is because 70% of the CFRP tendon strength was used for prestressing and the remaining 30% was used only for deflection during the cracking stage. Similarly, the 48% prestressed beam fails in higher deflection than the 61% prestressed beam.

Deflections of beams by the ACI 440.4R-04 method and Abdelrahman and Rizkalla's[9] method were compared with experimental results (Fig. 2). These comparisons revealed that both methods of deflection calculation underestimate the experimental deflection value. The deflection error by these methods was large when the deformability index of a beam was smaller. The ACI 440.4R-04 maximum least square error method, compared with the experimental result (*DI* equal to 1.35), is 103.44. Hence, the deflection models for FRP beams using the ACI 440.4R-04 and Abdelrahman models need modification to match the experimental results.

Abdelrahman and Rizkalla's experimental investigation revealed that the nonlinear deflection curve between the uncracked and cracked stages varies in relation to the percentage of prestressing for beams with similar specifications that had the same percentage of CFRP tendon area. Further, 50% prestressed beams perform better in deformation than 70% prestressed beams. The influence of these deformability parameters on the load–deflection curve may lead to shifts in the cracking moment and cracked moment of inertia of members at failure load and the nonlinear deflection curve pattern changes between the uncracked and cracked stages.

## Influence of effective moment of inertia $I_{eff}$ in deflection

Sunnal[10] et al. proposed an improved Branson and Trost[11,12] equation for the effective moment of inertia by using the reinforcement ratio and bond strength. They added two additional rational parameters $\alpha$ and $\beta$ to reduce the moment of inertia.

$$I_{eff} = \left(\frac{M_{cr}}{M_n}\right)^3 \frac{I_g}{\beta} + \left[1 - \left(\frac{M_{cr}}{M_n}\right)^3\right] \alpha I_{cr}$$

where

$M_{cr}$ = cracked moment of resistance

$M_n$ = moment of resistance at ultimate load

$I_g$ = gross moment of inertia

$I_{cr}$ = cracked moment of inertia

Khalfalla[13] also proposed two additional rational parameters $\Psi_1$ and $\Psi_2$ to reduce the moment of inertia.

$$I_{eff} = \left(\frac{M_{cr}}{M_n}\right)^3 \Psi_1 I_g + \left[1 - \left(\frac{M_{cr}}{M_n}\right)^3\right] \Psi_2 I_{cr}$$

ACI 440.4R-04 has recommended an additional factor $\beta_d$, allowing for the nonductile behavior of the CFRP bar to soften the moment of inertia values.

$$I_{eff} = \left(\frac{M_{cr}}{M_n}\right)^3 \beta_d I_g + \left[1 - \left(\frac{M_{cr}}{M_n}\right)^3\right] I_{cr}$$

$$\beta_d = 0.5\left(\frac{E_p}{E_s} + 1\right)$$

where

$E_p$ = Modulus of elasticity of CFRP

$E_s$ = Young's modulus of steel

If $E_p$ equals $E_s$, then $\beta_d$ equals 0.5(1 + 1) or 1, which is similar to the steel tendon $I_{eff}$ equation.

The ACI 440.4R-04 method of effective moment of inertia value depends on the factor $\beta_d$, and it is derived based on steel Young's modulus property. The moment curvature interaction of beams prestressed with FRP tendons is influenced by deformability, whereas the moment curvature interaction of beams prestressed with steel tendon is influenced by ductility. The ratio of deformability of FRP tendons to ductility of steel tendons is not a unique relationship in terms of Young's modulus. Further, the deformability of specific types of FRP tendons changes with the percentage of prestressing and modulus of rupture of concrete, but the ductility of steel is constant. Hence, this ACI 440.4R-04 rational approach does not provide any technical justification for calculating the deflection.

## Influence of neutral axis shift in deflection

Branson and Trost assessed the effect of prestressing eccentricity due to shift of neutral axis when a beam is in the cracking stage. It leads to an increase in prestressing moment and reduces the deflection's rate of increase. The shift of the neutral axis is nonlinear and varies with respect to member stiffness and the tension stiffening effect of concrete due to the prestressed tendon.

Abdelrahman and Rizkalla studied this effect for FRP prestressed beams. They suggest that the shift of the effective neutral axis distance of the beam from the extreme compression fiber during the cracking stage $Y_{eff}$ with respect to $M_{cr}/M_n$ happens more slowly than with steel tendons. This leads to a slower increase in prestressed moment. They proposed the shift of the neutral axis distance related to the square of $M_{cr}/M_n$ based on experimental test results.

$$Y_{eff} = \left(\frac{M_{cr}}{M_n}\right)^2 Y_g + \left[1 - \left(\frac{M_{cr}}{M_n}\right)^2\right] Y_{cr}$$

where

$Y_g$ = neutral axis distance measured from extreme compression fiber of beam until first crack in concrete

$Y_{cr}$ = neutral axis distance at ultimate stage

**Proposed mathematical model** Past research predicted that changes to the deflection pattern during the cracking stage are related to the deformability behavior of FRP bars, the percentage of prestressing, and the shift of the neutral axis during the concrete cracking stage considering the fully bonded member. The following mathematical deflection model is proposed considering various researchers' recommendations:

- Vogel, and Svecova[14] observed that the pattern of curves of $I_{eff}$ and $Y_{eff}$ with respect to $M_{cr}/M_n$ are not irregular deviations and follow the same pattern of curve, even under the influence of several parameters.

- Borosnyoi and Balazs[15,16] suggested that the deformability behavior of FRP tendon and the bond strength between the concrete and FRP tendon influences the deflection behavior of FRP prestressed beams.

Hence, a numerical analysis was conducted by considering the pattern of $I_{eff}$ and $Y_{eff}$ curves by varying the exponents $a$ and $b$ to study the deflection behavior of CFRP-based prestressed concrete beams. A new mathematical deflection model proposed based on the literature study is as follows.

$$I_{eff} = \left(\frac{M_{cr}}{M_n}\right)^a I_g + \left[1 - \left(\frac{M_{cr}}{M_n}\right)^a\right] I_{cr}$$

$$Y_{eff} = \left(\frac{M_{cr}}{M_n}\right)^b Y_g + \left[1 - \left(\frac{M_{cr}}{M_n}\right)^b\right] Y_{cr}$$

Exponents $a$ and $b$ for $I_{eff}$ and $Y_{eff}$ curves are related to the deformability and bond strength of the FRP tendon.

**Numerical analysis** The experimental results of specimen CFB4-1-H-0.7 were selected to describe the numerical method for calculating the optimum $a$ and $b$ values. Trial values between 3 and 6 were selected for exponent $a$ and between 1 and 3 for exponent $b$. The values of $a$ and $b$ were considered at intervals of 0.1, and the deflection of the beam for each probable combination of $a$ and $b$ values was calculated. There are 341 trials of deflection values for each load increment, and the errors on each trial were calculated with respect to experimental results. The errors were either positive or negative values, so the least square error was calculated for each trial by squaring the maximum and minimum errors.

**Figure 3** shows plots of the least square deflection error values of all of the trials to assess the convergence of the lowest least square error. The error curve forms a convex convergence shape. The deflection error is converging to the experimental deflection results for the $I_{eff}$ curve pattern power coefficient $a$ value of 4.5 to 5.5 for all possible values of the $Y_{eff}$ curve pattern exponent $b$. The error depends on dual-function parameters $a$ and $b$. Hence, the Lagrange dual-function convex optimization method was used to predict the optimal solutions of exponents $a$ and $b$ for the global optimum least square deflection error value. Lagrange stated that there were many local minimum least square error values for the various combination values of $a$ and $b$, hence the lowermost boundary of least square error due to the dual function value of $a$ and $b$ (**Fig. 3**)

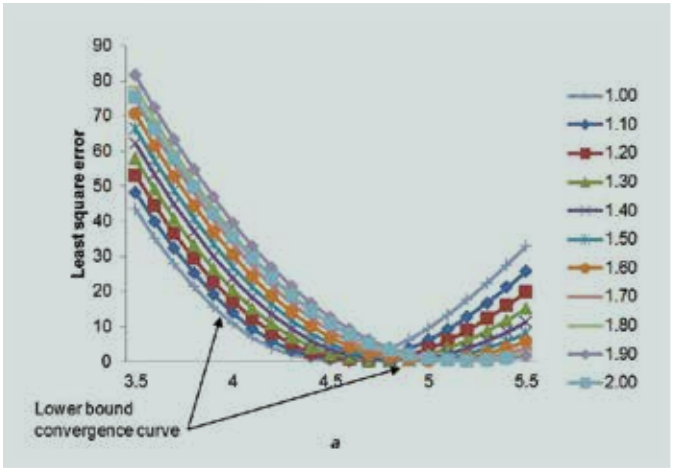


**Figure 3.** Least square error convergence for beam CFB4-1-H-0.7. Note: *a* = exponent.

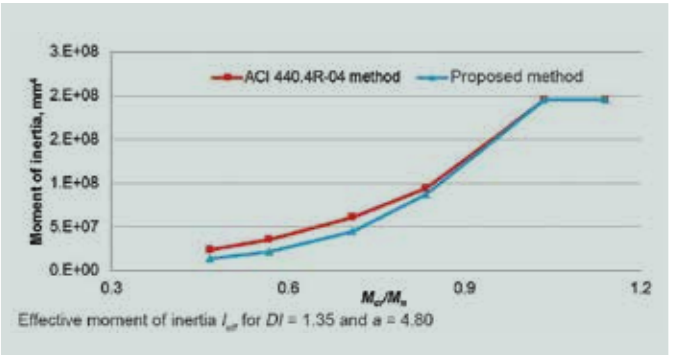


**Figure 4.** The effective moment of inertia curve for beam CFB4-1-H-0.7 is smoother than that given by the ACI 440.4R-04 method. Note: *a* = exponent; *DI* = deformability index; $I_{eff}$ = effective moment of inertia of member; $M_{cr}$ = cracked moment of resistance; $M_n$ = moment of resistance at ultimate load. 1 mm = 0.0394 in.

were detached from the source trails and then plotted the same with respect to the values of $a + b$. This least square curve was called the lower-bound convergence curve. The optimal values of *a* and *b* correspond to the average least square error in this convergence region (Fig. 3). The deflection of beam CFB4 was calculated with the proposed method using the optimal values of *a* and *b*. Figure 2 plots the load–deflection curve. A similar procedure was adopted for beams CFB1 to CFB3 and optimum values for *a* and *b*. The load deflection by the proposed method was plotted for beams CFB1 to CFB4 (Fig. 2). The proposed deflection calculation was compared with the ACI 440.4R-04 deflection method (Fig. 2). ACI 440.4R-04 method of calculating coefficient values of *a* equal to 3 and *b* equal to 2 led to erroneous deflections compared with the deflections from the experimental results and underestimated the actual deflection.

## Effective moment of inertia $I_{eff}$

The effective moment of inertia curve for beam CFB4-1-H-0.7 is smoother than that given by the ACI 440.4R-04 method (**Fig. 4**). The quicker shift of effective moment of inertia for the low-deformability-index FRP beam is due to most of the strain being used for prestressing the tendon and the balance of available strain only being used to deform during the cracking stage. Per the proposed method, the exponent is 4.80 instead of 3, as suggested in the ACI 440.4R-04 method.

$$I_{eff} = \left(\frac{M_{cr}}{M_n}\right)^{4.80} I_g + \left[1 - \left(\frac{M_{cr}}{M_n}\right)^{4.80}\right] I_{cr}$$

## Shift of neutral axis distance $Y_{eff}$

The shift in neutral axis distance for the beam CFB4-1-H-0.7 is less than that from the ACI 440.4R-04 method (**Fig. 5**). The slower shift of neutral axis is due to high-tension stiffening of the beam in the tensile zone during the cracked stage as a result of a high percentage of prestressing.

The exponent *b* is 1.3 instead of 2 as suggested by Abdelrahman's method.[9]

$$Y_{eff} = \left(\frac{M_{cr}}{M_n}\right)^{1.3} Y_g + \left[1 - \left(\frac{M_{cr}}{M_n}\right)^{1.3}\right] Y_{cr}$$

## Proposed *a* and *b* values

The numerical analysis as described was followed for beam specimens CFB1 to CFB4 and determined the optimum *a*

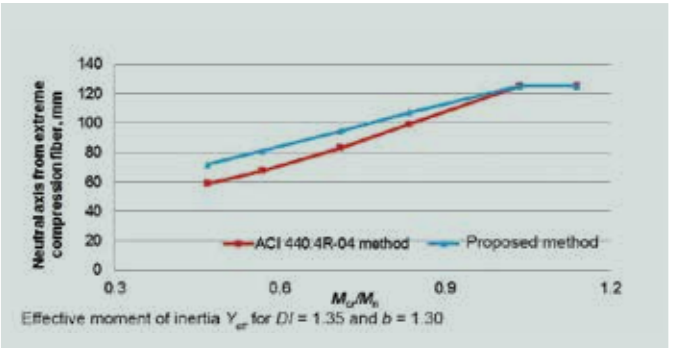


**Figure 5.** The neutral axis shift curve for beam CFB4-1-H-0.7 is slower than that given by the ACI 440.4R-04 method. Note: *b* = power coefficient; *DI* = deformability index; $M_{cr}$ = cracked moment of resistance; $M_n$ = moment of resistance at ultimate load; $Y_{eff}$ = effective neutral axis distance of member from extreme compression fiber during cracking stage. 1 mm = 0.0394 in.

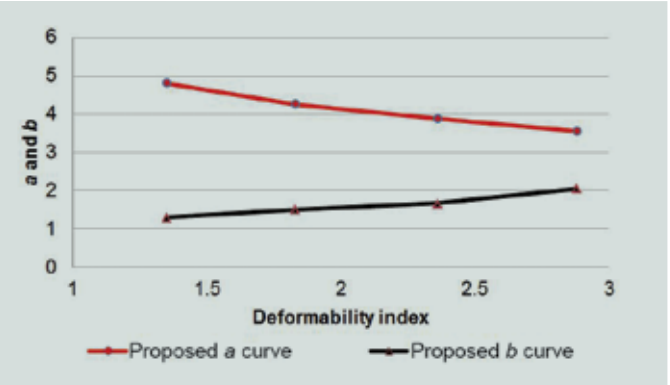


**Figure 6.** Design chart for exponents *a* and *b*.

and *b* values. Both exponents *a* and *b* change with respect to a member's deformability index value (**Fig. 6**). The optimal value of *a* is inversely proportional to the deformability index value of the member. The exponent *a* is larger at a low deformability index, which leads to a smoother curve than what results from the high deformability index. The high percentage of prestressing of an FRP tendon leads to less balanced strain of a CFRP tendon $\varepsilon_m$, where $\varepsilon_m$ equals $\varepsilon_{pu} - \varepsilon_{ps}$. The shift of effective moment of inertia is faster, leading to a faster increase in deflection and earlier final deflection than with a high deformability index.

The exponent *b* is directly proportional to the deformability index value. The exponent *b* is larger at high deformability index values, which leads to a faster rate of shift of neutral axis due to less of a stiffening effect due to low prestressing values.

The deflection based on experimental and numerical studies reveals that the deflection of CFRP prestressed beams is influenced by the beam's deformability behavior. Detailed numerical studies are required to calculate the effective moment of inertia and effective neutral axis distance by considering many experimental test sample results to refine the research and select optimum values for exponents *a* and *b*.

## Crack width

Experimental results showed that the concrete cracks were developed below the neutral axis in the constant moment zone in the region between the two point loads. The first cracks started near the middle of the support, and then further crack patterns developed. At a certain load, crack patterns stabilized and no new cracks developed as the load on the beam was increased. The existing cracks in the FRP beam increased in depth instead of forming new crack patterns.

Deng and Liang[17] stated that FRP-reinforced beams exhibit larger crack widths than beams reinforced with steel bars due to the low modulus of elasticity of FRP tendon. Similarly, larger crack widths were observed in the experimental results. Fewer cracks stabilized for the low-deformability-index beam than the high-deformability-index beam (**Fig. 7**). There are four crack patterns for the beam with *DI* equal to 1.35, whereas five crack patterns developed in the beam with *DI* equal to 2.88. The average crack spacing for the low-deformability-index beam was 323 mm (12.7 in.), which is larger than the high-deformability-index beam value of 258 mm (10.2 in.). Frosch[18] stated that the crack spacing of FRP tendons is greater compared with steel tendons due to the development of less stiffness at the bottom of the beam.

Weichen and Tan[19] stated that the crack stabilization load $P_{st}$ is reached more quickly for a low-deformability beam

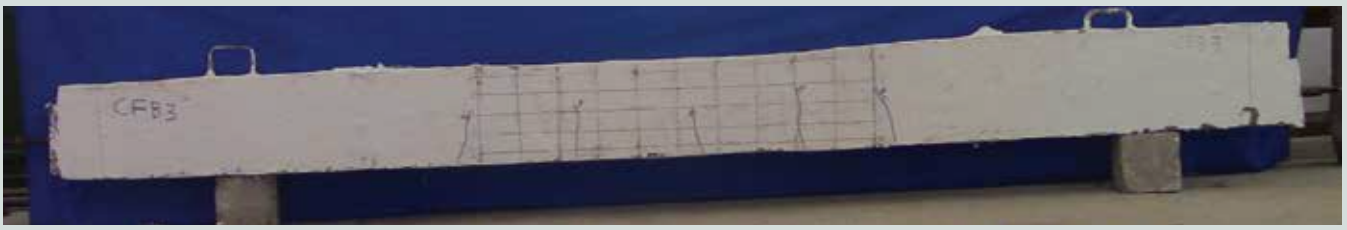


Beam CFB3-1-H-0.35

Beam CFB4-1-H-0.70

**Figure 7.** Crack patterns.

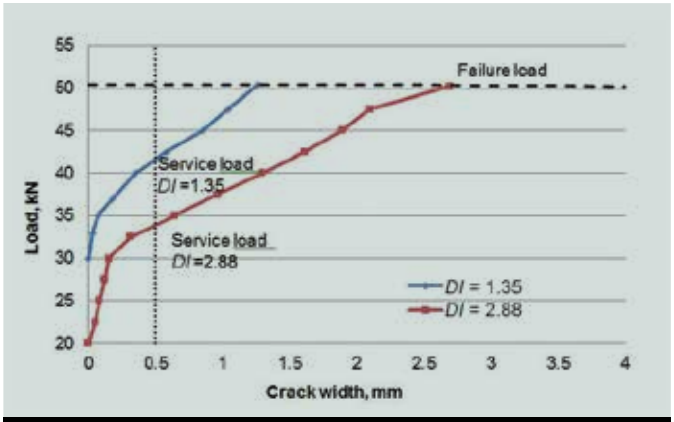


**Figure 8.** Crack width pattern of beams. Note: *DI* = deformability index. 1 mm = 0.0394 in.; 1 kN = 0.225 kip.

(**Fig. 8**) due to the high tensile stiffening of the concrete at the bottom surface in beams with a high percentage of prestress. The ratio of load at stabilized crack pattern to load at first crack is 1.1 for a low-deformability-index beam and 1.3 for a high-deformability-index beam. The high-deformability beam allows the stabilized crack pattern some time to settle due to the slow and steady rate of increase of strain in the FRP bar.

The crack pattern in Fig. 8 resembles the load–deflection curve pattern. The rate of cracking increases slowly up to the crack stabilization load and then increases linearly until failure. The high-deformability-index beam crack width is larger than that of the low-deformability-index beam.

Mertol et al.[20] stated that there is no durability requirement for allowable crack widths; however, it has to be restricted according to the serviceability considerations of the structure. CAN/CSA S806-02[21] recommends a permissible crack width of 0.5 mm (0.02 in.) to meet serviceability requirements. The service loads corresponding to a 0.5 mm crack width were calculated (Fig. 8). The service load $P_s$ of the high deformability beam is 1.57 times greater than the first crack load $P_{cr}$ (Fig. 8). For the low-deformability beam, $P_s/P_{cr}$ is smaller than for the high-deformability beam; however, the net service load is larger because the cracked load is larger compared with the low percentage of prestress. A detailed crack width study considering many test sample results is required with respect to the deformability behavior of FRP prestressed concrete beams.

## Conclusion

The following conclusions were drawn based on this study:

- The serviceability behavior of CFRP prestressed concrete beams is influenced by the deformability behavior of the beam.
- The proposed method is efficient for calculating the deflection of a CFRP prestressed concrete beam because it is based on the strain approach for calculating effective moment of inertia and shift of neutral axis distance. The proposed load–deflection curve is derived from experimental results.
- The balance strain $\varepsilon_m$ on a CFRP bar after prestressing determines the effective moment of inertia of a beam during the cracking stage. Hence, greater available balance strain leads to greater beam deformability, resulting in larger beam deflection and crack width.
- The prestressing strain $\varepsilon_{ps}$ and bond strength of concrete decide the rate of shift of the neutral axis during the cracking stage of a beam. The prestressing strain $\varepsilon_{ps}$ induces additional tension stiffening, which slows down the rate of shift of neutral axis for the fully bonded beam. Higher prestressing strain leads to a slower rate of shift of neutral axis. The resistance effect of prestressing moment is slower due to the slow rate of increase of eccentricity, which leads to lesser deflection and crack width at ultimate load.
- The shift of moment of inertia of an FRP-based prestressed concrete beam is faster compared with a steel-based prestressed concrete beam due to faster crack stabilization. Crack stabilization of FRP prestressed beams is faster for low-deformability-index beams than for high-deformability-index beams; hence, it leads to more crack spacing and less crack patterns for the low deformability index beam. Therfore, a low-deformability-index beam reaches faster service load at a 0.5 mm (0.02 in.) crack width than a high-deformability-index beam.
- Based on the study described in this article, the authors conclude that deflection, crack width, crack spacing, crack pattern, and crack stabilization are influenced by the deformability behavior of fully bonded FRP prestressed beams.
- Detailed experimental and numerical studies of the serviceability behavior of beams, considering a larger number of experimental test samples, are required to validate this proposed model.

## Acknowledgments

The authors are grateful to R. Bala Subramanian, Pierre Hofmann, and the management of Dextra Building Products (Guang Dong) Co. Ltd. in Guangzhou, China, for providing CFRP material to conduct experimental testing; G. Mohan Kumar and M. Suchetha for their support in conducting the research presented in this paper; and Mark

Richard Barnett, manager of Egis Rail in England, for reviewing this paper.

## References


1. Burke, C. R., and C. W. Dolan. 2001. "Flexural Design of Prestressed Concrete Beams Using FRP Tendons." *PCI Journal* 46 (2): 76–87.

2. Burke, C. R., and C. W. Dolan. 1996. "Flexural Strength and Design of FRP Prestressed Beams." In *Proceedings of the Advanced Composite Materials in Bridges and Structures-2nd International Symposium Canadian Society of Civil Engineers*, pp. 383–393. Montreal, QC, Canada: Canadian Society for Civil Engineering.

3. American Concrete Institute (ACI) Committee 440. 2004 (reapproved 2011). *Prestressing Concrete Structures with FRP Tendons*. ACI 440.4R-04. Farmington Hills, MI: ACI.

4. Burgoyne, C. J. 2001. "Ductility and Deformability in Beams Prestressed with FRP Tendons." In *FRP Composites in Civil Engineering: Proceedings of the International Conference on FRP Composites in Civil Engineering*, 1:15–25. Amsterdam, Netherlands: Elsevier.

5. Johnson, S. 2011. "Prestressed BFRP Tendons in Concrete Beam." MS thesis, Reykjavík University.

6. Schmidt, J. W., B. Taljsten, A. Bennitz, and H. Pedersen. 2009. "FRP Tendon Anchorage in Post Tensioned Concrete Structure." In *Concrete Repair, Rehabilitation and Retrofitting II*, 1181–1186. Leiden, Netherlands: CRC Press/Balkema.

7. Tadros, M., A. Ghali, and A. Meyer. 1985. "Prestress Loss and Deflection of Precast Concrete Members." *PCI Journal* 30 (1): 114–141.

8. Swanson, Derek, and C. W. Dolan. 2002. "Development of Flexural Capacity of a FRP Prestressed Beam with Vertically Distributed Tendons." *Composites Part B* 33 (1): 1–6.

9. Abdelrahman, A., and S. Rizkalla. 1999. "Deflection Control of Concrete Beams Pretensioned by CFRP Reinforcements." *Journal of Composite Construction* 3 (2): 55–62.

10. Al-Sunna, R., K. Pilakoutas, P. Waldron, and T. Al-Hadee. 2006. "Deflection of FRP Reinforced Concrete Beams." In *Proceedings of 2nd International Congress on International Federation of Structural Concrete FIP Congress*, Naples, Italy: *fib* (International Federal for Structural Concrete).

11. Branson, D. E., and H. Trost. 1982. "Application of the I-Effective Method in Calculating Deflections of Partially Prestressed Members." *PCI Journal* 27 (5): 62–67.

12. Branson, D. E. 1968. "Design Procedures for Computing Deflections." *Journal of the American Concrete Institute*, no. 65: 730–742.

13. Khalfallah, S. 2009. "Explaining the Riddle of Effective Moment of Inertia Models for FRP Concrete Beams." Paper presented at First International Conference on Sustainable Built Environment Infrastructures in Developing Countries, ENSET, Oran, Algeria.

14. Vogel, H., and D. Svecova. 2009. "Effective Moment of Inertia Expression for Concrete Beams Reinforced with Fiber Reinforced Polymer (FRP)." Paper presented at ACI Convention, San Antonio, TX.

15. Borosnyoi, A. 2010. "Bond of Carbon Fibre Reinforced Polymer (CFRP) Prestressing Tendons in Concrete—Multiparameter Laboratory Studies." *Journal of Epites-Epiteszettudomany*, no. 38: 95–120.

16. Borosnyoi, A., and G. L. Balazs. 2002. "Prestressing Provided by CFRP Tendons." *Journal of Concrete Structures*, no. 3: 75–80.

17. Deng, Yu, and Jiong Feng Liang. 2011. "Deflection and Crack Width Prediction of Partially Bonded CFRP Concrete Beams." *Advanced Materials Research*, no. 168: 2182–2185.

18. Frosch, R. J. 1999. "Another Look at Cracking and Crack Control in Reinforced Concrete." *ACI Structural Journal*, no. 96: 437–442.

19. Xue, Weichen, and Yuan Tan. 2012. "Cracking Behavior and Crack Width Predictions of Concrete Beams Prestressed with Bonded FRP Tendons." In *Proceedings of the 6th International Conference on Composites in Civil Engineering*. Rome, Italy: International Institute for FRP in Construction. https://www.iifc.org/publications/proceedings-iifc-official-conferences/cice-2012-rome-italy-13-15-june-2012/.

20. Mertol, H. C., S. Rizkalla, P. Scott, J. Lees, and R. El-Hacha. 2006. "Durability of Concrete Beams Prestressed with CFRP." Paper presented at Special Session—Subcommittee 440I for FRP Prestressed Concrete, ACI Fall Convention, Denver, CO.

21. CSA (Canadian Standards Association). 2002. *Design and Construction of Building Components with Fibre-Reinforced Polymers*. CAN/CSA S806-02. Toronto, ON, Canada: CSA.

## Notation

$a$ = exponent

$A$ = area of carbon-fiber-reinforced polymer tendon

$b$ = exponent

$d$ = effective depth

$DI$ = deformability index

$E_c$ = Young's modulus deformability index of concrete

$E_p$ = Young's modulus of carbon-fiber-reinforced polymer tendon

$E_s$ = Young's modulus of steel

$f_c^{'}$ = compressive strength of concrete

$I_{cr}$ = cracked moment of inertia of member

$I_{eff}$ = effective moment of inertia of member

$I_g$ = gross moment of inertia of member

$k$ = ratio of neutral axis depth to effective depth

$L$ = length of the carbon-fiber-reinforced polymer tendon

$M_{cr}$ = cracked moment of resistance

$M_n$ = moment of resistance at ultimate load

$P$ = prestressing load

$P_{cr}$ = load at first crack

$P_s$ = service load

$P_{st}$ = load at crack stabilization stage

$Y_{cr}$ = neutral axis distance of member from extreme compression fiber at cracked stage

$Y_{eff}$ = effective neutral axis distance of member from extreme compression fiber during cracking stage

$Y_g$ = centroid of member from extreme compression fiber

$\alpha$ = rational parameter

$\beta$ = rational parameter

$\beta_1$ = stress block factor for concrete

$\beta_d$ = softening factor

$\delta$ = total elongation of tendon and stud

$\delta_1$ = elongation of stud

$\delta_2$ = elongation of carbon-fiber-reinforced polymer tendon

$\delta_3$ = elongation of stud

$\varepsilon_m$ = balance strain of carbon-fiber-reinforced polymer tendon after prestressing

$\varepsilon_{ps}$ = prestressing strain of carbon-fiber-reinforced polymer tendon

$\varepsilon_{pu}$ = ultimate strain of carbon-fiber-reinforced polymer tendon

$\rho$ = reinforcement ratio

$\Psi_1$ = rational parameter

$\Psi_2$ = rational parameter

## About the authors


P. Selvachandran, PhD, is a research scholar in the Department of Civil Engineering at Kongu Engineering College, Perundurai, Erode, Anna University, India.

S. Anandakumar, PhD, is a professor and head of the Department of Civil Engineering at Kongu Engineering College, Perundurai, Erode, Anna University, India.

K. L. Muthuramu, PhD, Charter Engineer, is a professor and head of Shanmuganathan Engineering College, Pudukkottai, Anna University, India.


## Abstract


An experimental investigation was conducted to study the influence of deformability behavior in carbon-fiber-reinforced polymer (CFRP) prestressed concrete beams. The moment curvature of CFRP prestressed beams does not follow the linear stress–strain curve, showing that there is some amount of energy absorbed, which influences the serviceability behavior of members. Four beam specimens were cast, stressed at deformability index values varying from 1.35 to 2.88, and tested. Numerical analysis was conducted using the experimental results. It was concluded that the deformability of beam influences the serviceability behavior of the beam and proposed new deflection model. The proposed model is an efficient method for calculating deflection compared with the ACI 440.4R-04 method. A design chart is suggested for calculating effective moment of inertia and effective neutral axis distance. The influence of the deformability index in crack width, crack spacing, number of crack pattern, and crack stabilization load are also described.


## Keywords


Carbon-fiber-reinforced polymer, CFRP, crack stabilization load, crack width, deflection, deformability, effective moment of inertia, effective neutral axis.


## Review policy


This paper was reviewed in accordance with the Precast/Prestressed Concrete Institute's peer-review process.


## Reader comments

Please address reader comments to journal@pci.org or Precast/Prestressed Concrete Institute, c/o *PCI Journal*, 200 W. Adams St., Suite 2100, Chicago, IL 60606.